# Chapter A

# SOAR AO: system analysis and simulation

Prepared by: *A. Tokovinin*
Version: 1.1
Date: March 24, 2003
File: AOsimul.tex

## A.1 Turbulence sensing and compensation methods

### A.1.1 Classical AO with natural guide stars

The SOAR telescope is destined to reach high angular resolution in the visible part of the spectrum. Adaptive optics (AO) is a natural way to achieve this goal, but the obstacles to visible-light AO are formidable and well known: lack of suitably bright natural guide stars (NGSs), cone effect for laser guide stars (LGSs), small corrected field. On the other hand, low-order AO systems designed for IR are known to improve image quality in the visible as well, shrinking the size of partially corrected image by as much as two times (e.g. PUEO at CFHT). Hence, the idea to improve (enhance) visible-light seeing at SOAR by means of AO emerged in 2001. Such a system could potentially improve SOAR performance for a wide variety of astronomical programs. The gain in the PSF parameters under partial compensation is plotted in Fig. A.1 (Tokovinin, 2001, unpublished). It remains significant in the regime $d/r_0 = 4...10$, where the Strehl ratio is practically zero.

The PUEO AO system has sub-aperture size around 1 m and can use guide stars up to R=15-16. Partial correction is achieved in a field of view not more that 1 arcmin diameter around the NGS. Sky coverage of such system can be considerable at low Galactic latitudes, but it remains low near Galactic poles. Moreover, the size of the compensated field is not large and the uniformity of compensation over the field is poor.

### A.1.2 Multi-conjugate AO

It is possible to widen the corrected field by means of Multi-Conjugate Adaptive Optics (MCAO), such as being developed for Gemini-S. However, SOAR has a modest 4-m aperture, and when a FOV of

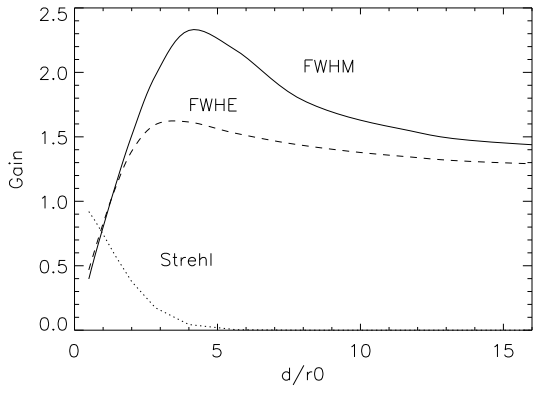


Figure A.1: Gain in the size of residual image halo, (FWHM, full line), and its half-energy diameter (FWHE, dashed line), as a function of the ratio of actuator spacing to $r_0$. Strehl ratio is plotted as dotted line. For $d/r_0 < 4$ image energy goes into diffraction limited core, while the remaining halo is wider than in the partial compensation regime, $d/r_0 > 4$.

several arcminutes is being corrected, the foot-prints of the beam do not overlap in high atmospheric layers. In these conditions MCAO is not efficient: to correct the 3D turbulent volume with several DMs, information on turbulence distribution is obtained by tomography with several NGSs, and beam overlap is an important condition for this method to work. With several NGSs few arcminutes apart, we can only measure effectively the ground-layer turbulence.

### A.1.3 Ground layer correction with multiple NGSs

Studies of the turbulence vertical profile at Cerro Pachón have shown that most turbulence is indeed concentrated near the ground. Correction of the ground layer only would result in image quality improvement in a wide field [6]. Thus, it seemed attractive to explore the idea of ground layer correction with several NGSs. If 3 suitably bright NGSs are found in a FOV of 3-5 arcmin., such correction is indeed possible. This idea is confirmed by Monte-Carlo simulations of M. Chun [2]. He used the same turbulence profile as in our simulations and found that with three R=12 stars a uniform partial correction of the FOV of $3'$ diameter is achieved, atmospheric FWHM of $0\farcs56$ is improved to $0\farcs3$.

The density of bright stars is low. In order to reach significant sky coverage, realistic magnitudes of those NGSs will be around R=15. For example, Le Louarn et al. [4] give the sky coverage of 10% at Galactic pole and 100% at lower latitudes for $15^m$ stars and $6'$ diameter FOV. With such faint NGSs we can correct only the elements of no less than 1 m across, so that only part of ground-layer turbulence can be compensated. The gain in the FWHM brought by partial ground layer compensation with NGSs turns out to be quite modest. Roughly, FWHM improvement by partial compensation of all layers is about 2 times, FWHM improvement by full compensation of ground layer alone is also about 2 times, so under those two conditions FWHM can be improved by only about 25%. Somewhat better results can be achieved in dense stellar fields where brighter NGSs are available (e.g. in LMC or in Galactic plane), but this would restrict the general usefulness of the AO system.

### A.1.4 Ground layer correction with Rayleigh LGS

Rayleigh laser guide stars are known to be insensitive to high atmospheric layers. They are a natural choice for ground layer correction, offering considerably better performance than NGSs. Given the favorable characteristics of modern solid-state lasers, LGS-based AO can be even simpler than a system with several NGSs. When LGS is placed at low altitude, the WFS signal contains only low-layer

perturbations, and the uniformity of AO correction over the field improves. This has actually been confirmed with an LGS at 10 km altitude using the Starfire Optical Range facility [1]. A low-altitude LGS gives high return flux, easing requirements on the laser.

Any LGS requires additional tip-tilt measurements on natural guide stars because tilts of LGS are corrupted by upward propagation. If only one NGS is selected for t-t correction, the t-t signal will contain contributions from all layers, so the uniformity of compensation will be affected. We propose to use several (2-4) t-t stars distributed around the science field in order to isolate the t-t contribution from lower layers and hence to improve the compensation uniformity.

Independently of our effort, ground layer compensation with Rayleigh LGS was proposed for the WHT 4.2 m telescope by Rutten et al. [8]. The goal of their system will be to maximize light concentration in $0\farcs3$ pixels of an imaging spectrometer OASIS, leaving aside the concerns of correction uniformity over FOV. For that reason they prefer to put LGS at an altitude of 15 km. Simulations done by that group (using a different turbulence profile) confirm the expected resolution gain: atmospheric FWHM of $0\farcs74$ (R-band) is reduced to $0\farcs32$ with LGS and a t-t NGS of R=18 at $1'$ off-axis.

Classical AO compensation with a bright NGS and a narrow field is a first step of the SOAR AO project. This HR mode has its own value, provided that NGS limit is not too bright. Achievable compensation quality as a function of NGS magnitude is also evaluated in our simulations.

We studied various options outlined above with a modal covariance code [10] developed for MCAO analysis (Sect.A.2). The performance on NGS was checked with a Monte-Carlo simulation that is more realistic and takes into account temporal loop response and CCD readout noise. (Sect. A.3). Analysis of sky coverage with LGS and plans for further simulations are presented in Sects. A.4 and A.5, respectively.

## A.2 Simulation with modal code

### A.2.1 Simulation tools

We estimated the AO performance using the modal covariance code [10]. The routine for PSF computation along the lines of Véran et al. [11] was added. Briefly, the phase structure function of the compensated wave-front is computed as a difference between the atmospheric structure function (for von Kàrmàn turbulence model with finite outer scale) and the effect of compensation, computed from the covariances of Zernike modes and the "mode shape functions". The optical transfer function is then found as a product of the diffraction-limited OTF and the atmospheric term. Strehl ratio and Fried resolution are computed by direct integration of the OTF. It is verified that high Strehl ratios match their values given by Marechal approximation. The Fourier transform of the OTF leads to the PSF, for which various metrics are determined.

Temporal aspects are not included into the simulation: all measurements and corrections are instantaneous. In real life, some contribution of the servo lag should be added. However, the photon flux from the GSs is computed for 1 ms exposure time, while in reality the closed-loop bandwidth is not likely to exceed 100 Hz. Hence, the magnitude limits are approximate and likely pessimistic. The performance of a real AO system is expected to be slightly better for faint GSs and slightly worse for bright GSs.

Table A.1: Seeing at Cerro Pachón (at zenith)

| Probability | 25% (good) | 50% (median) | 75% |
|---|---|---|---|
| Fried parameter at 0.5 $\mu$m, cm | 20.0 | 15.0 | 10.7 |
| Standard FWHM at 0.5 $\mu$m, arcsec | 0.50 | 0.67 | 0.94 |
| Finite-outer-scale FWHM at 0.5 $\mu$m, arcsec | 0.40 | 0.55 | 0.79 |
| Finite-outer-scale FWHM at 2.2 $\mu$m, arcsec | 0.24 | 0.33 | 0.49 |

Note: at zenith distance of 45° seeing degrades by a factor of 1.23.

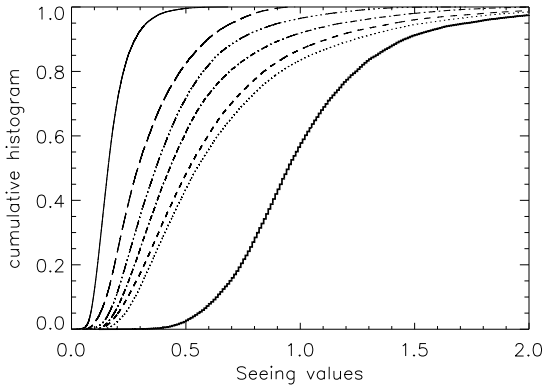


Figure A.2: Cumulative distribution of the total seeing (thick line) and (from right to left) of the seeing that would result from correction of the ground layer below 0.5 km, first 1 km, first 2 km, etc. to the seeing produced by the 16 km layer alone (leftmost curve) [13]. These data were obtained at Cerro Tololo, but the characterization of the high atmosphere should be valid for Cerro Pachón.

### A.2.2 Atmospheric conditions at Cerro Pachón

Data on seeing at Cerro Pachón obtained during the Gemini campaign in 1998 [12] are summarized in Table A.1. Compared to standard optical atmospheric propagation theory, we take into account

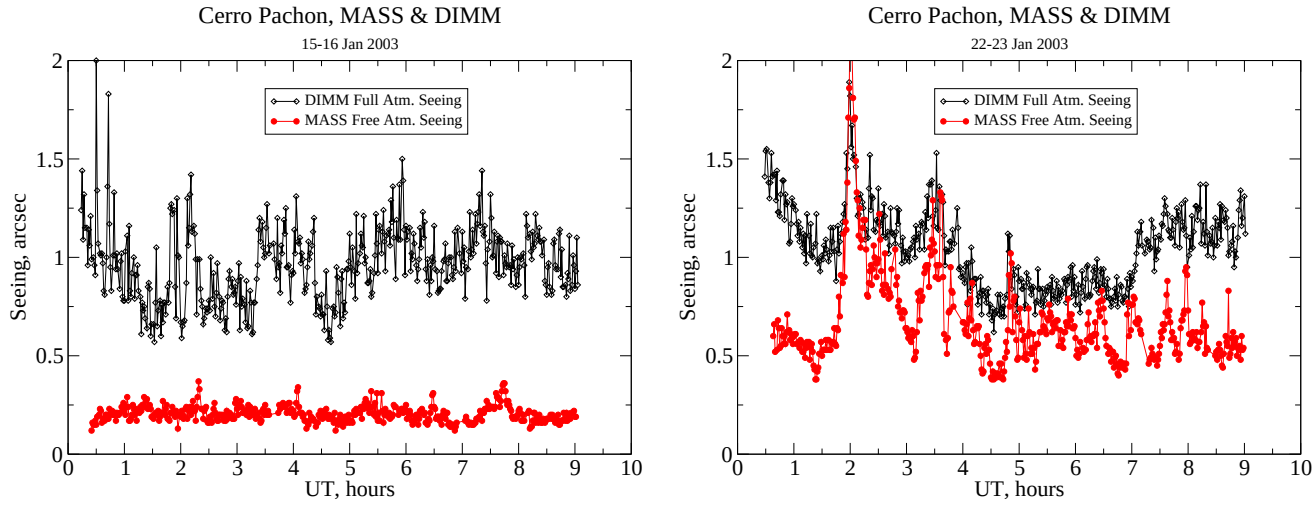


Figure A.3: Seeing as a function of time for two nights at Cerro Pachón: calm night (left) and bad night (right). Seeing in the free atmosphere (red line, dots) was measured by the MASS turbulence profiler, total seeing (black line, diamonds) was measured by a DIMM monitor located at 1.5 m above ground.

the finite outer scale of turbulence, as actually measured at Cerro Pachón. This leads to a smaller seeing limited PSF (for a given turbulence integral or given $r_0$) and to a faster improvement of seeing at longer wavelengths, compared to the standard theory. This is in large measure due to a decrease in the amplitude of image motion when the outer scale is taken into account. Thus the standard theory over-estimates the relative gain to be obtained from tip-tilt correction alone.

In the simulations, the mean vertical turbulence profile is approximated by 7 layers at altitudes from 0 to 15.8 km, with the ground layer containing 65% of the total turbulent energy; this is the same model used for the Gemini MCAO simulations [3] and in [2]. Different seeing conditions were simulated by changing the intensity of all layers while keeping their relative strengths fixed.

The turbulence profile is in fact highly variable, so the size of the compensated field and achievable seeing improvement are also variable. Extensive statistics of turbulence profile at the nearby mountain Cerro Tololo was collected in May-September 2002 (some 20000 measurements over 58 nights) [13]. Although local conditions at Cerro Tololo and Cerro Pachón are different, the upper atmosphere should be the same, hence the relevance of these data to SOAR AO. This study generally confirms the results of Vernin et al. [12] and shows that in 60% of cases the ground layer below 0.5 km indeed contributes 0.6 of total turbulence power. The histograms of upper-atmosphere seeing given in Fig. A.2 should not be interpreted directly as a prediction for ground-layer compensation, however. The situation is a little more complicated because the ground layer is compensated only partially by a realistic AO system, but, on the other hand, some partial compensation of high layers is achieved as well (cf. [6]).

Seeing produced by the "free atmosphere" $\epsilon_f$ (all layers above 0.5 km) is, generally, more stable than total seeing. There exist periods of calm atmosphere as long as 4 days when $\epsilon_f$ is stable at the level of $0\farcs2$–$0\farcs3$. Those periods correspond to jet stream wind velocities in the range 20-30 m/s. Given that wind speed can be predicted few days ahead, we can forecast AO-favorable conditions and use these forecasts in planning of observations. Examples of good and bad nights at Cerro Pachón are given in Fig. A.3. Although total seeing on both nights was quite similar, around $1''$, ground-layer compensation would improve image quality by a factor of 5 on January 15 and would bring little gain on January 22.

### A.2.3 System parameters

Table A.2: Parameters of tip-tilt and two AO modes for median seeing

| Option | Zernike compens. | Sub-apert. | Guide stars | FOV | FWHM (0.5 $\mu$m) |
|---|---|---|---|---|---|
| Tip-tilt | 2,3 | 4.2 m | 1 NGS, $5^m - 17^m$ | $2' - 3'$ | $0\farcs50$ |
| HR mode | 2-66 | 0.4 m | 1 NGS, $5^m - 12^m$ | $10''$ | $0\farcs03$ |
| LR mode | 2-66 | 0.4 m | 1 LGS, 10 km | $3'$ | $0\farcs35$ |

The main parameters of the SOAR AO system as input into the simulations are listed in Table A.2; we assume that 66 Zernike modes can be compensated. For LGS, it is assumed that the tip-tilt signal is available, whereas in practice it will be obtained from several off-axis NGSs. For comparison, we also estimate the performance of tip-tilt compensation using the same atmospheric model. In fact, compensation quality achieved with tip-tilt and one guide star degrades at angular distance of $> 1'$ from the GS, hence the useful field of view (FOV) is loosely estimated to be $2' - 3'$. It is possible

to improve the uniformity (at the expense of reduced resolution gain) by using three tip-tilt stars instead of one, but this capability is not implemented in any of the SOAR instruments, hence it is not considered here.

The estimates given here assume that the telescope is ideal. Although everything is being done to assure that SOAR will take full advantage of the excellent seeing at Cerro Pachón, the AO system can help correct any residual telescope aberrations. In this more realistic case, the gain from using AO will be increased, as compared to our predictions. On the other hand, telescope vibrations and high-frequency polishing defects on optics will reduce the performance. At a later stage, realistic telescope parameters will be included in the simulations.

By compensating 66 Zernike modes with a bright NGS, a Strehl ratio of 0.06 can be achieved at 0.5 $\mu$m in median seeing, increasing to 0.16 under good seeing. At 0.8 $\mu$m, Strehl ratios are 0.35 and 0.52, respectively. The diffraction-limited FWHM is $0\farcs034$ and $0\farcs046$ at 0.5 and 0.8 $\mu$m.

### A.2.4 Variation of PSF over the field

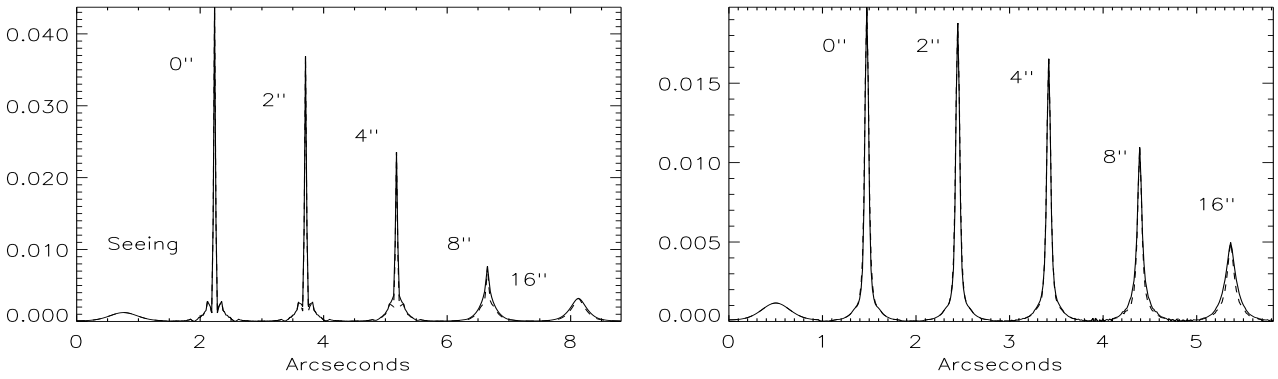


Figure A.4: Stacked PSFs on-axis and at increasing distance from the guide star in high resolution mode. Seeing-limited PSF is plotted first for comparison. Left: median seeing, 0.5 $\mu$m, bright NGS. Right: good seeing, 0.66 $\mu$m, $12^m$ NGS.

In HR mode, the PSF changes over a $10''$ field are already dramatic (Fig. A.4). It is evident, however, that even at low Strehl ratios, the diffraction-limited core is very prominent, favoring deconvolution.

In LR mode, the resolution gain is modest, because high atmospheric layers are not properly sensed with a Rayleigh LGS. On the other hand, and for the same reason, the compensated field is much larger, with a very uniform PSF over the whole field. The PSFs in Fig. A.5 were computed for an LGS altitude of 8 km. Under good seeing, the FWHM at 0.66 $\mu$m improves from $0\farcs37$ to $0\farcs21$ ($1^m$ gain in the central pixel intensity). Better resolution gain can be achieved at the expense of compensated field if the LGS is placed at 20 km. Under good seeing, moving LGS from 10 to 20 km improves FWHM at 0.66 $\mu$m from $0\farcs21$ to $0\farcs075$. At 0.8 $\mu$m, a FWHM of $0\farcs07$ becomes possible (Strehl ratio 12%, gain in the intensity of central pixel $2.6^m$).

The objectives of the seeing improvement mode are very similar to those which motivated the implementation of tip-tilt for SOAR first light. However, both the resolution gain and PSF uniformity offered by the seeing-improved mode are better than for tip-tilt compensation (Fig. A.5). The resolution gain from tip-tilt compensation is less than originally anticipated because turbulence outer

scale is now taken into account. Furthermore, variation of the tip-tilt corrected PSF over the 5′ FOV is significant and becomes even more dramatic in conditions when the resolution gain is greatest (K-band, good seeing). Such a variable PSF poses significant problems in data reduction and may affect the photometric precision.

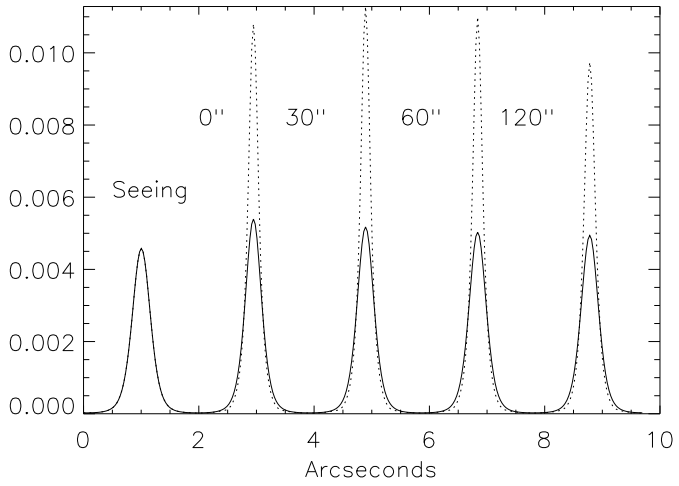


Figure A.5: Stacked PSFs on-axis and at increasing distance from the guide star for tip-tilt compensation (full line) and for seeing-improved AO (dotted line). Uncorrected seeing-limited PSF is plotted first. Good seeing, 0.66 $\mu$m wavelength.

### A.2.5 Limiting magnitude in HR mode

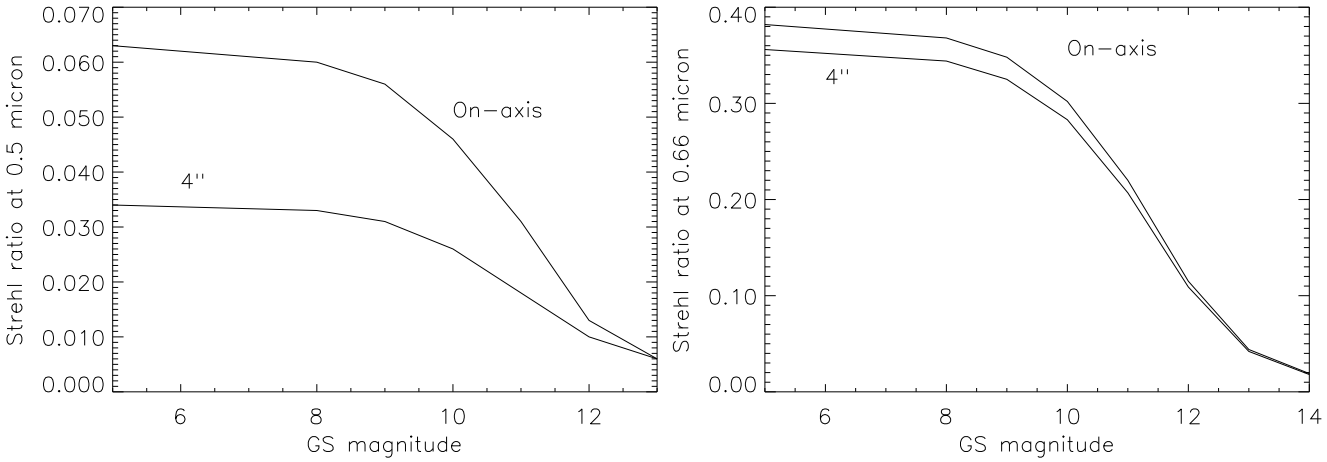


Figure A.6: Strehl ratio on-axis and at 4″ offset as a function of NGS R magnitude in high-resolution mode. Left: 0.5 $\mu$m, median seeing. Right: 0.66 $\mu$m, good seeing ($r_0 = 20$ cm).

How faint a star can be used as an NGS in HR mode? In Fig. A.6 (left) the Strehl ratio at 0.5 $\mu$m is plotted against NGS magnitude. Note that with a bright NGS, better Strehls could be achieved for compensation orders higher than 66. Alternatively, when the NGS is too faint (e.g. $15^m$), the compensation order can be reduced; the Strehl ratio will then be very low, but some seeing improvement will still be obtained.

Much better performance will be possible under good seeing and at longer wavelengths. In Fig. A.6 (right), the astrophysically important case of observations in the R band is presented. Even with

guide star as faint as $12^m$, diffraction-limited imaging in a $10''$ field is possible. The uniformity of compensation over the field is also better in this case.

### A.2.6 Gain in FWHM

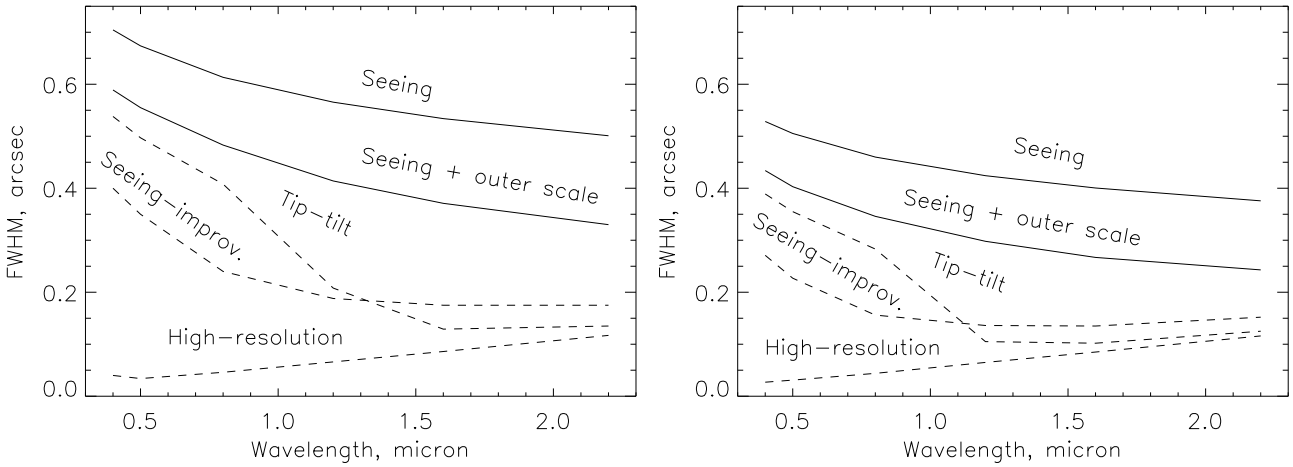


Figure A.7: The FWHM as a function of wavelength for median seeing ($r_0 = 15$ cm, left) and for good seeing ($r_0 = 20$ cm, right). The two solid curves correspond to uncompensated images with infinite outer scale (standard theory) and with an outer scale of 25 m. The dashed lines trace the FWHM for the tip-tilt (on-axis), improved seeing mode with Rayleigh LGS and high resolution mode with a NGS.

The FWHMs of uncompensated and compensated images as a function of wavelength are given in Fig. A.7. The influence of a finite outer scale is very noticeable. The outer scale of 25 m is typical for Cerro Pachón and other top class sites [12]. However, it varies considerably with time and may be either larger (e.g. 50-200 m) or smaller (15 m), so the actual atmospheric image size will be somewhere between the two curves. For a large outer scale, the amplitude of tip and tilt increases, hence the gain brought by tip-tilt and AO is larger.

In HR mode, the FWHM is diffraction limited at all wavelengths (on-axis), although the Strehl ratio in the visible is low. The FWHM gain in LR mode at 0.5 $\mu$m is 35% for median seeing and 46% for good seeing.

Please, note that the FWHM of uncompensated images in the K band is already $0\farcs25$ under good seeing and $0\farcs33$ under median seeing; it improves at long wavelengths faster than $\lambda^{-0.2}$ due to outer scale effects. A telescope with perfect optics, without turbulence in the dome and without wind shake, should be able to achieve this performance (as seems to be the case at Gemini S).

### A.2.7 Gain in Strehl ratio and encircled energy

The Strehl ratio is the most common metric of AO performance. In Fig. A.8 (left) the gain in the equivalent characteristic (Fried resolution) is plotted. It corresponds to the gain of the light intensity in the center of the PSF compared to the "standard" uncompensated atmospheric PSF (infinite telescope, infinite outer scale). The gain is expressed in magnitudes. In the right panel, the FWHE (Full Width at Half Energy) diameter is plotted. Gains in FWHE are less than those in FWHM: while AO decreases

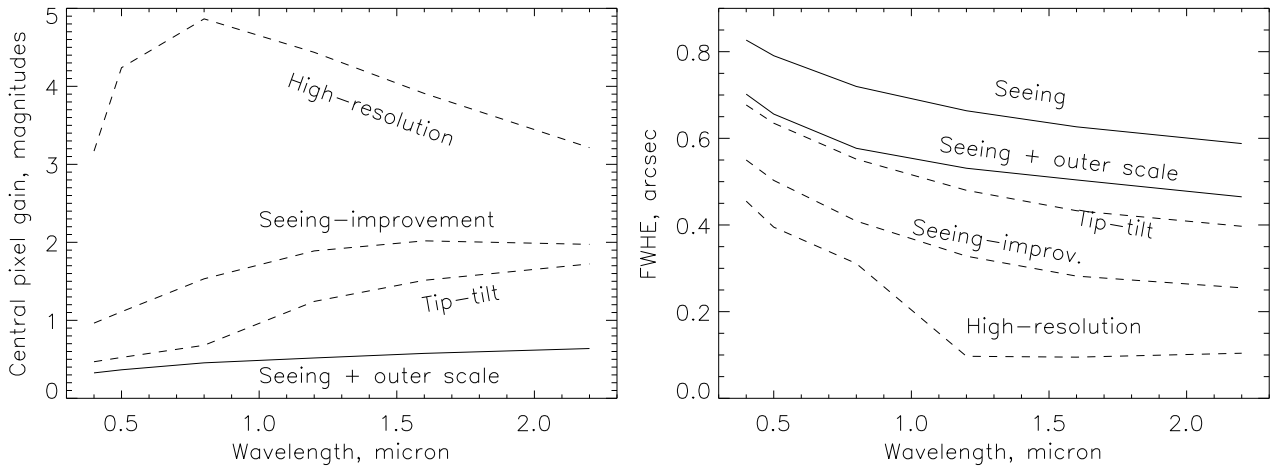


Figure A.8: The gain in light intensity at the PSF center (in magnitudes) is plotted on the left as a function of $\lambda$ for median seeing. For uncompensated images (solid curve), the gain is due to the outer scale effect. On the right, the diameter containing half the encircled energy, FWHE, is plotted for median seeing.

the size of the PSF, its structure is also changed compared to the atmospheric PSF, developing a narrow core while leaving considerable energy in the wings.

## A.3 Monte-Carlo simulation of HR mode

### A.3.1 Method and input data

We wanted to confirm the results obtained by the modal covariance code with another, complementary code based on Monte-Carlo emulation of an AO system. The code `simul.pro` was written by F. Rigaut (version of March 2001) and was downloaded from the web [5].

The specific goal of this study was the comparison in WFS performance between curvature and Shack-Hartmann (S-H). In the SOAR AO project, achievement of diffraction-limited resolution *in the visible* with the faintest natural guide stars is one of the goals. The behavior of these two WFSs at low light levels can be significantly different. First, S-H WFS is usually associated with CCD detectors and, hence, with some readout noise (RON). What level of RON can be tolerated and to what extent is it critical for achieving faint GS magnitudes? Secondly, noise propagation properties of S-H and curvature WFSs are different: curvature systems produce more noise at low spatial frequencies (low-order modes like tip-tilt) which may destroy the coherence of compensated wavefronts at the scale of aperture, leading to an enlargement of the central peak in the compensated image. On the other hand, curvature systems are more effective at high spatial frequencies, and thus the compensated wavefronts can be more smooth, with a better coherence at short spatial scales and better concentration of energy in the compensated image.

Our atmospheric model corresponds to median seeing conditions at Cerro Pachón: $r_0 = 0.15$ m at 500 nm. The imaging wavelength is fixed to 700 nm, or $D/r_0 = 18.9$ for a telescope diameter $D = 4.25$ m. The vertical distribution of turbulence and its time constant are not changed with respect to the original Rigaut code: 5 layers at altitudes of 0, 1.6, 3.6, 6.3, and 11.6 km above telescope, relative intensities 0.18, 0.28, 0.18, 0.19, 0.17, wind speeds 3, 10, 15, 25, 15 m/s. Only the

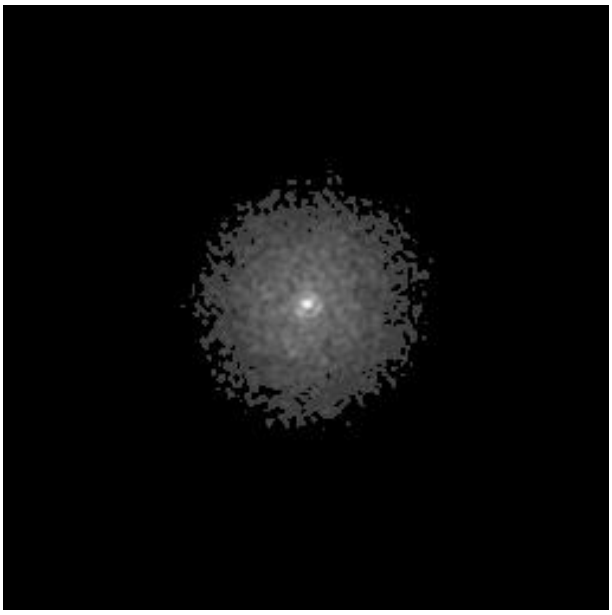

Example of the PSF simulated with the Rigaut's code. Curvature AO system, bright NGS, median seeing, imaging wavelength 600 nm. The intensity stretch is adjusted to show the seeing halo.

time constant is relevant here, because we do not study anisoplanatism.

The calculation of stellar flux assumes that the total number of photons per second detected by the WFS from the whole telescope aperture is equal to $Fe^{-0.5m}$, where $m$ is the R-magnitude of the GS, and $F$ is the zero point. We take $F$= 1.36000e+11, assuming a total efficiency of 40% and a spectral bandpass of 300 nm, as recommended in the Roddier book [7]. The last assumption is probably optimistic, because stellar photons may be shared between WFS and scientific channel. Real magnitude limits may thus be some 1 mag. brighter.

The command matrix used in the code is obtained by a simple singular-value decomposition (SVD) inversion of the interaction matrix. Better results would be achieved with an optimized command matrix that automatically reduces compensation order for faint GSs while trying to minimize the residual phase variance. Optimization will improve limiting magnitudes, but it has not yet been tried.

The code computes Strehl ratio (SR) for the long-exposure compensated image after a certain number of loop iterations (we chose 150 iterations, the first 20 are skipped). Also, a short-exposure SR is computed as an average of instantaneous SRs. This second parameter is higher, being insensitive to residual image motion and also being enhanced by the speckle structure of the stellar image. We use the short-exposure SR only for comparison with "real" long-exposure SR. An example of the averaged PSF is given in Fig. A.3.1.

### A.3.2 Shack-Hartmann system

We suppose that the DM is capable of compensating 66 Zernike modes. This is an approximation to the yet-unspecified curvature DM. Using Noll formulas, the theoretical residual phase would be 1.04 rad$^2$, or Strehl ratio (SR) of 0.35 (here and below all values are given for the imaging wavelength of 700 nm). If the efficiency of the AO system (in the sense of Roddier) is not ideal, and instead of radial order 10 it compensates only up to radial order 8 (45 modes), the expected residual would be 1.46 rad$^2$, SR=0.23 (without WFS noise and time lag).

We assume a geometry of 10x10 square apertures across pupil diameter, or 72 useful apertures inside pupil. Several modes are rejected in the inversion of the interaction matrix. Our basic choice

is a S-H WFS with 2x2 pixels per sub-aperture working in a quad-cell mode. This is motivated by reduction of read-out noise (RON), and is the solution adopted in Keck and Gemini AO systems. We found that even with a short loop time of 1 ms and bright GS of 5 mag. (no influence of RON), a SR of only 0.15 could be achieved, and some residual motion of the compensated image was apparent. The reason must be related to the quadrant S-H mode which has an inherent noise related to the changing image structure at individual sub-apertures. When an artificial source blur was introduced, we obtained SR=0.20. Finally, with a S-H of 9x9 pixels per sub-aperture (pixel size $0.26''$) we obtained SR=0.24. Increasing loop time to 2 ms leads to SR=0.17.

Our basic 2x2 pixel mode with 2 ms loop time thus gives sub-optimal performance for bright GSs. We still adopt these parameters for the study of limiting magnitudes. A curve of SR versus R-magnitude is given in Fig. A.9 left.

### A.3.3 Curvature system

For the curvature system, we adopted the geometry of the 79-actuator electrostatic DM from Okotech. We did not attempt any optimization of geometry at this stage and assumed that the pupil border is projected at the inner radius of the last ring of electrodes. Taking this radius as 1, the relative radii of the rings are 0.19, 0.40, 0.59, 0.79, 1.0, 1.26. Corresponding numbers of electrodes are 1, 7, 14, 21, 28, 8. The central obscuration of the telescope is 0.15. The WFS geometry is matched to the DM geometry; the saturation of DM is not modeled.

The value of defocusing $l$ (the stroke of membrane mirror) is a critical parameter, to be adapted to NGS magnitude and seeing. In the simulation code, a beam f-ratio of $F/D$ =1:60 is always assumed. The formula 5.12 of the minimum $l$ from the book [7] is

$$l > \left(\frac{F}{D}\right)^2 \frac{D}{d} D\theta_B, \tag{A.1}$$

where $d = 0.4$ m is sub-aperture diameter and $\theta_B = 0.5''$ is the beam blur. This leads to $l > 0.37$ m. We tried the $l$ values of 0.15 (originally in the code example, adopted for PUEO), 0.2 and 0.3. All these choices work for bright GSs, and with $l = 0.15$ we obtained SR=0.21 for a bright R=5 NGS. On the other hand, with $l$ this small the loop is not closed for R=13 star, whereas better results are obtained with $l = 0.2$. We adopted $l = 0.3$ for our simulations reported below. There is no penalty in fast loop, because RON is zero for curvature systems. The loop time was set to 1 ms.

### A.3.4 Comparison of the two systems

Fig. A.9 gives the comparison of the S-H and curvature systems. It is seen that the S-H system gives lower SR for bright stars. However, this is due to a longer loop time and additional noise in a 2x2 WFS, as explained above. If these two defects are corrected, we obtain SR=0.24 and FWHM of 35 mas - slightly better than for a curvature system.

As for the limiting magnitude, both systems show a very similar performance. Pending the optimization of the command matrix and of the S-H centroid computation (thresholding), it is difficult to name a winner. Considering that S-H is conceptually simple, will work with an extended pulsed source (LGS), is cheaper and easier to maintain, we selected this WFS concept for further study.

**Conclusions:**

1. It seems reasonable to expect diffraction-limited resolution with a S-H WFS with 4e RON and NGS of R=12...13, even without optimization of the command matrix.

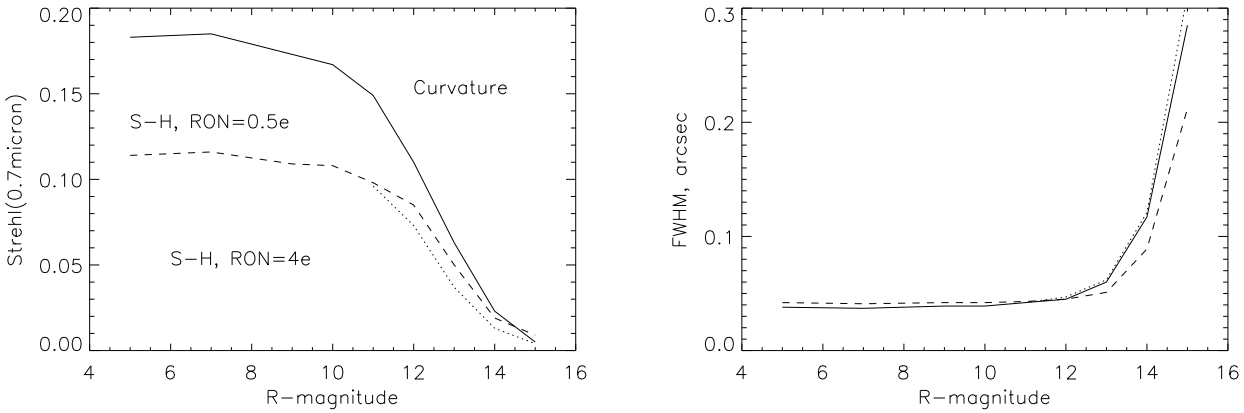


Figure A.9: Strehl ratio (left) and FWHM (right) against guide star R-magnitude. Full line: curvature system, 1 ms loop. Dashed line: S-H system, 2 ms loop, 2x2 pixel/subap. WFS, RON=0.5e. Dotted: same, RON=4e.

2. In order to reach the Strehl ratio limited by compensation order, we need a loop time of 1 ms and a S-H design with more than 2 pixels per sub-aperture.

## A.4 Tip-tilt guiding and sky coverage in LR mode

### A.4.1 Requirements for tip-tilt error

Up to three tip-tilt (t-t) guide stars are needed in LR mode for tip-tilt correction, in order to isolate the ground layer contribution and to make t-t correction isoplanatic. We have to select those stars outside the $3'$ diameter of the science field but not too far from it. We set the outer diameter of the patrol field as $5'$. The surface of the annular patrol zone is the same as the surface of a $4'$ diameter circular field. Will there be enough t-t stars in this zone to ensure complete sky coverage in LR mode? How faint will those stars be?

The t-t tracking will be needed only in LR mode, when the PSF size is improved but still much larger than the diffraction limit. This relaxes requirements compared to normal AO systems. Suppose that the profile of the compensated PSF is approximated by a Gaussian curve with FWHM=0.″3 and corresponding dispersion $\sigma_0 = \mathrm{FWHM}/2.35 = 128$ mas. If the rms dispersion of tilt is $\sigma_t$, the resulting PSF will have a dispersion $\sqrt{\sigma_0^2 + \sigma_t^2}$. Let us require that tip-tilt error do not degrade the intensity of the central pixel in the PSF (equivalently, Strehl ratio, although this criterion has little meaning in LR mode) by more than 10%. This leads to the condition

$$\frac{1}{\sigma_0^2 + \sigma_t^2} > 0.9 \frac{1}{\sigma_0^2}, \tag{A.2}$$

or $\sigma_t < 0.316\sigma_0 = 40$ mas.

### A.4.2 Estimate of flux and limiting magnitude

As a detector for t-t, we consider either a quadrant photomultiplier (R5900, Hamamatsu) or photon-counting APDs, like in the WYIN tip-tilt system or in curvature AO systems. Assuming that the latter have quantum efficiency of 0.8, that the transmission of atmosphere, telescope and optics is 0.5 and that the total spectral band is 300 nm, the total detected flux from R=15 star will be 1.36 $10^5$ photoelectrons/s for 4.25 m SOAR aperture. The flux detected by the PMT will be ∼4 times less because of its lower quantum efficiency.

There is no need to track tip-tilt very fast, 10 Hz bandwidth will be adequate. Wind velocity in the ground layer will not be very high. Even assuming $V = 20$ m/s (fast enough to close the dome), wave-front will travel 2 m in 100 ms. Thus, the loop frequency of t-t servo system can be as low as 100 Hz. An R=18 starwill give $N = 86$ photons per loop cycle, permitting to measure stellar position with a rms error of $\sigma N^{-1/2} = 30$ mas, where the rms spread of uncorrected image is assumed to be $\sigma = 285$ mas for $0''.67$ FWHM seeing. Averaging t-t signals from three stars will reduce rms error to 17 mas. The actual error will 5.4 mas – less by a factor of $\sqrt{10} = 3.16$ because it is determined by the closed-loop bandwidth rather than by the loop cycle time.

An error of 40 mas will be reached for stellar flux of 50 photons (combined from 3 stars and per 100 ms time) that corresponds to three R=22.3 stars in case of APD detectors or R=20.8 in case of PMT. For stars this faint, we have to take into account sky background, which has not been done yet.

The estimates given above might appear too optimistic when compared to the practice of other telescopes. At Gemini the guide probes are limited to about R < 15. This happens because Gemini operates loop at 1 kHz and closed-loop bandwidth is over 100 Hz, compensating for wind shake. Moreover, the readout noise of fast CCD detectors dominates the errors at low fluxes. A more relevant comparison is provided by the PUEO AO system which uses APDs. PUEO with its 1 m sub-apertures works with stars down to R=16; same flux with 4.25 m aperture will be obtained for R=19.1. Given that PUEO AO loop is faster than our t-t loop, that its error budget is tighter that in SOAR AO LR mode, and that only one star instead of 3 is used in PUEO, our estimate of R=22.3 limit with APDs is confirmed.

The mechanical structure of SOAR telescope is very rigid, so wind-induced vibrations should be small. If it turns out that vibrations are indeed a problem, a faster t-t loop should be implemented with correspondingly brighter limiting magnitude of guide stars. Final requirements to SOAR AO t-t system will be formulated after measurements of the SOAR telescope vibration spectrum. Use of a seismometer [9] may be considered as a way to off-load vibrations from the tip-tilt guider and to increase the limiting magnitude.

### A.4.3 Sky coverage

Probability to find a given number of stars obeys Poisson law. If $\mu$ is the average number of stars per field, the probability to find three or more stars $P(3)$ is

$$P(3) = 1 - \exp(-\mu)(1 + \mu + \mu^2/2). \tag{A.3}$$

This curve is plotted in Fig. A.10. In order to find three or more stars in 80% of fields (i.e. sky coverage 80%), we need on the average 4.3 stars per field.

According to various sources, the average number of stars brighter than R=18 in a $4'$ diameter field at Galactic pole (Galactic latitude $b = 90°$) is 3.9. The number of stars brighter than a given magnitude R increases roughly as $10^{0.25R}$, so the 80% coverage will be reached for R=18.2 limiting

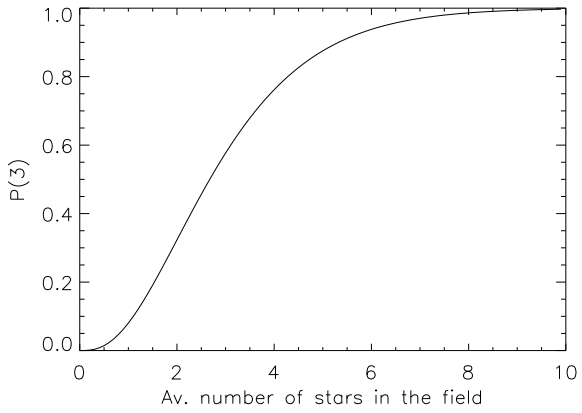


Figure A.10: Probability to find three or more stars $P(3)$ as a function of the average number of stars in the field.

magnitude. At lower Galactic latitudes guide stars will be significantly brighter, e.g. the same 80% coverage will be reached for R=14.2 at $b = 0°$ and for $R = 16$ at $b = 30°$.

The analysis of sky coverage shows that there is a sufficient freedom for selecting t-t stars. Even when using PMTs as light detectors, we still have a resource of 2.6 magnitudes (10 times in flux) even at Galactic pole. This resource can be used either to increase the sky coverage beyond 80% or to do a faster guiding.

## A.5 Plans for further system simulation

The system analysis presented above is preliminary. More simulations are planned to characterize the future SOAR AO system and to find design trade-offs.

**Tip-tilt trade-offs in LR mode.** The tip-tilt guiding was not actually simulated in the modal code: it was supposed that LGS provides valid tip-tilt. This will be rectified. We want to investigate the influence of the number and configuration of guide stars on the system performance. Given that atmospheric tilts are small (owing to finite outer scale), an option without t-t compensation will be considered as well.

**Wider set of conditions.** So far, we calculated the performance only for the average turbulence profile and for zenith viewing. Now turbulence profile statistics has been studied much better, so we shall define several typical turbulence profiles and study the performance of the system in each case, both at zenith and for different zenith angles.

**WFS optimization.** We want to explore the best centroiding techniques in S-H WFS, to estimate the potential gain brought by using the L3 CCDs with internal amplification, to evaluate the pyramid WFS concept that, according to several authors, can increase the NGS magnitude limit by as much as one magnitude.

**Saturation of the DM.** Simulations are needed to evaluate the impact of finite DM stroke on the compensation quality.

# Bibliography


[1] Chun M., The useful field of view of an adaptive optics system. 1998, PASP, 110, 317-329

[2] Chun M., Gains from ground-only adaptive optics system. 2003, Proc. SPIE, 4839, 94-98

[3] Ellerbroek, B. L. & Rigaut, F. 2000, in Adaptive Optical Systems Technology, ed. P. L. Wizinovich, Proc. SPIE, 4007, 1088

[4] Le Louarn M., Hubin N., Sarazin M., and Tokovinin A., New challenges for Adaptive Optics: Extremely Large Telescopes, Mon. Notices Roy. Astron. Soc., 317, 535-544, 2000.

[5] Rigaut F., AO simulation code. 2001, http://babkock.ucsd.edu/cfao_ucsd/ao_simulate.html

[6] Rigaut F., New varieties of Adaptive Optics. in: *Beyond Conventional Adaptive Optics,* eds. Vernet E., Ragazzoni R., Esposito S., Hubin N., ESO Conf. Proc., 2002, 58, 11-16.

[7] Roddier F, ed., Adaptive optics in astronomy, Cambridge Univ. Press, Cambridge, 1999.

[8] Rutten R.G.M., Clark P., Myers R.M. et al., 2003, Proc. SPIE, 4839, 360-369

[9] Tokovinin A., Pendular seismometer for correcting telescope vibrations. Mon. Notices Roy. Astron. Soc., 2000, 316, 637-641.

[10] Tokovinin A., Le Louarn M., Viard E., Hubin N., Conan R., Optimized modal tomography in Adaptive Optics. Astron. Astrophys., 2001, 378, 710.

[11] Véran J.-P., Rigaut F., Maître H., Rouan D., Estimation of the adaptive optics long-exposure point-spread function using control loop data, JOSA (A), A14, 3057 (1997).

[12] Vernin J., Agabi A., Avila R., Azouit M., Conan R., Martin F., Masciadri E., Sanchez L., and Ziad A., Gemini site testing campaign. Cerro Pachon and Cerro Tololo, *Gemini RPT-AO-G0094, http://www.gemini.edu/*, 2000.

[13] Tokovinin A., Baumont, S., Vasquez J. Statistics of turbulence profile at Cerro Tololo. MNRAS, 2003, accepted. See also astro-ph/0209432